

# Quantification of Cellular Properties from External Fields and Resulting Induced Velocity: Magnetic Susceptibility

Jeffrey J. Chalmers,<sup>1</sup> Seungjoo Haam,<sup>1,\*</sup> Yang Zhao,<sup>1</sup> Kara McCloskey,<sup>1</sup> Lee Moore,<sup>2</sup> Maciej Zborowski,<sup>2</sup> P. Stephen Williams<sup>3</sup>

<sup>1</sup>Department of Chemical Engineering, The Ohio State University, 140 WEST 19th Avenue, Columbus, Ohio 43210; telephone: +1 (614) 292-2727; fax: +1 (614) 292-3769; e-mail: Chalmers.1@osu.edu

<sup>2</sup>Department of Biomedical Engineering, The Cleveland Clinic Foundation, 1900 Euclid Avenue, Cleveland, Ohio 44195

<sup>3</sup>Department of Chemistry and Geochemistry, Colorado School of Mines, 1500 Illinois Street, Golden, Colorado 80401

Received 17 May 1998; accepted 11 January 1999

**Abstract:** An experimental technique is discussed in which the magnetic susceptibility of immunomagnetically labeled cells can be determined on a cell-by-cell basis. This technique is based on determining the magnetically induced velocity that an immunomagnetically labeled cell has in a well-defined magnetic energy gradient. This velocity is determined through the use of video recordings of microscopic images of cells moving in the magnetic energy gradient. These video images are then computer digitized and processed using a computer algorithm, cell tracking velocimetry, which allows larger numbers ( $>10^3$ ) of cells to be analyzed. © 1999 John Wiley & Sons, Inc. *Biotechnol Bioeng* **64**: 519–526, 1999.

**Keywords:** magnetic susceptibility measurements; computer imaging; immunomagnetic labeling; magnetic cell separation

## INTRODUCTION

The ability to analyze and/or separate cells based on the presence of specific molecules, either on the surface or within the cell, is a significant tool with applications ranging from fundamental biological studies to clinical practice. The development of the technology that allows these analyses and separations to be conducted has occurred in conjunction with the significant advances that have been made in the development of specific cellular probes. The sophistication of these probes led to the increasing knowledge of cellular processes. In many ways, it is the joint development of the technology and the fundamental understanding that have contributed to the current state of knowledge of the field.

The list of properties/characteristics that can be analyzed exceeds the objective of this paper; however, examples include total protein content, cellular pigment content, intra-

cellular pH, membrane organization, DNA content, and probably the most important characteristic from a clinical point of view, the presence of specific surface receptors or clusters of differentiation (CD) such as CD 4, CD 8, CD 34, etc. on lymphocytes (Shapiro, 1995).

The fundamental bases of these analytical and separation instruments are 2-fold: the ability to label the specific cell of interest with the probe, and the ability to either detect or differentiate the cell with the bound probe from the rest of the cells in the suspension. In the case of cell separation, this bound probe is used as a “handle” to separate the labeled cell from the other cells in the suspension.

## Specific Cellular Probes

A variety of labels are used in a number of different technologies. The most specific labels are those that bind only to a narrow class of cell associated molecules. While a number of these highly specific labels exist, i.e., streptavidin, the most commonly used labels are antibodies. These antibody labels are then usually covalently linked to a molecule, a particle, or a support matrix.

## Analytical Instruments

Analytical use of the cell labels range from qualitative fluorescence microscopic studies to the much more highly quantitative fluorescence activated cell scanning (FACS) systems. A second and much simpler analytical device is one which uses paramagnetic particles covalently bound to antibodies (Winto-Morbach et al., 1994, 1995, 1996). A further discussion of this device will be given below.

## Separation Instruments

A number of commercial separation systems exist based on immunological interactions. These can be grouped into immunofluorescent, immunomagnetic, and immunosolid/immunomatrix categories. The most common immunofluorescent cell separation system is the sorting version of the FACS system mentioned previously. A number of commercial, immunomagnetic separation technologies exist (MPC

\* Present address: Chemical Engineering Department, Yonsei University, 134 Shinchon-Dong, Seodaemoon-Ku, Seoul 120-752, Korea

Correspondence to: J. J. Chalmers

Contract grant sponsors: National Science Foundation; National Institutes of Health; Whitaker Foundation

Contract grant numbers: BCS 9258004; CA 62349; 20010308

separator series, Dynal AS, Trondheim, Norway; MACS system, Miltenyi Biotec GmbH, Bergisch Gladbach, Germany; Magnetic Separation System, Immunicon Corp. Huntington Valley, PA). The applications of these magnetic separation systems run from basic biological and biotechnological applications, such as the selection of specific clones to the treatment of human disease, such as the isolation of human stem cells (Gee et al., 1989; Miltenyi et al., 1990; Radbruch et al., 1994; Busch et al., 1994; Schmitz et al., 1994). Commercial applications of immunosolid/immunomatrix separations include the attachment of the specific antibody to the bottom of a vessel (immunopanning) (Gard et al., 1996; Madison et al., 1996) and the attachment of the specific antibody to packing material within a column (CEPRATE, CellPro Inc. Bothell, WA) (Bertolini et al., 1997; Collins et al., 1997; Vogel et al., 1996).

Since the focus of this paper is on the use and applications of immunomagnetic labels, the remainder of the paper will focus on this topic. Immunomagnetic labels can be classified into three groups based upon the size of the paramagnetic compound: particulate (on the order of a cell diameter, typically 1–5  $\mu\text{m}$ ), colloidal (on the order of 100 nm), and molecular (on the order of 10 nm). A number of particulate and colloidal immunomagnetic labels can be purchased commercially (Dynal AG; Miltenyi Biotec GmbH; Immunicon Corp.) while the third, molecular, is available from research labs (Zborowski et al., 1995). With respect to work presented in this paper, two important points need to be made: (1) the magnetic moment of a paramagnetic label is proportional to its volume; consequently, particulate paramagnetic labels exert orders of magnitude higher forces on a cell than colloidal or molecular; (2) with the smaller immunomagnetic labels, the potential exists to create a proportionality between the force exerted on a labeled cell and the number of cell surface markers.

Since most cells are not intrinsically paramagnetic and are usually diamagnetic (Chalmers et al., 1998a), unlike the intrinsic cell fluorescence of cells observed in FACS systems, greater than 3 orders of magnitude in difference between magnetically unlabeled and labeled cells are theoretically possible when colloidal or molecular labels are used. If it is assumed that a one-to-one correspondence exists between the cell surface marker number and the number of paramagnetic labels bound to a cell, then it is theoretically possible to impart a range of at least 3 orders of magnitude of magnetization to labeled cells (with well-characterized surface markers) compared to unlabeled cells.

### Mathematical Relationship Defining Immunomagnetically Induced Velocity

As was discussed in a previous report (Chalmers et al., 1998a), the fundamental forces acting on an aqueously suspended, paramagnetically labeled cell are magnetic, buoyant force, gravity and drag, designated,  $\mathbf{F}_m$ ,  $\mathbf{F}_{\text{bou}}$ ,  $\mathbf{F}_g$ , and  $\mathbf{F}_d$ , respectively. Assuming a Reynolds number less than

1.0, one can assume that  $\mathbf{F}_d$  is represented by Stokes drag. Mathematically, these forces are expressed by

$$\mathbf{F}_m = A_c \alpha \beta \mathbf{F}_b, \quad (1)$$

$$\mathbf{F}_g - \mathbf{F}_{\text{bou}} = \frac{(\rho_c - \rho_f) \pi D_c^3 g}{6}, \quad (2)$$

$$\mathbf{F}_d = -v_c 3 \pi D_c \eta, \quad (3)$$

where  $A_c$  is the surface area of the cell,  $\alpha$  is the number of cell surface markers per membrane surface area,  $\beta$  is the number of antibody magnetic bead complexes bound per cell surface marker,  $\mathbf{F}_b$  is the magnetic force acting on one antibody magnetic bead complex,  $D_c$  is the diameter of a cell,  $g$  is the acceleration of gravity,  $v_c$  is the magnetically induced velocity of a cell,  $\rho_f$  is the density of the fluid,  $\rho_c$  is the density of a cell, and  $\eta$  is the viscosity of the fluid. It is assumed in this derivation that the binding of immunomagnetic labels does not affect the cell volume or density. While the relationship for  $\mathbf{F}_m$  appears relatively straightforward,  $\mathbf{F}_b$  is highly nonlinear (except under specialized conditions) and expressed by

$$\mathbf{F}_b = \Delta\chi V_b \nabla \mathbf{B}^2 / 2\mu_o, \quad (4)$$

where  $\mu_o$  is the magnetic permeability of free space,  $\Delta\chi$  is the difference in magnetic susceptibility between the magnetic bead,  $\chi_b$  and the surrounding medium,  $\chi_f$  (saline in this case),  $V_b$  is the volume of one magnetic bead, and  $\mathbf{B}$  is the external magnetic field (Zborowski, 1997). (Note that  $\mathbf{F}_b$  is a vector in the direction of magnetic energy gradient.)

In a previous publication (Reddy et al., 1996), we discussed a method to determine the magnetic susceptibility of Dynabeads and 20- $\mu\text{m}$  latex beads. In this case, instead of discrete paramagnetic beads attached to the surface of a cell (or particle), as indicated in Eq. (1), it was assumed that the entire particle was paramagnetic. This assumption corresponds to an expression for the paramagnetic force on a cell (or particle) which is similar to Eq. (4):

$$\mathbf{F}_m' = \Delta\chi_c V_c \nabla \mathbf{B}^2 / 2\mu_o, \quad (5)$$

except the volume of a paramagnetic bead,  $V_b$ , is replaced with the volume of the paramagnetically labeled cell (or particle),  $V_c$ , and the difference in the magnetic susceptibility between a paramagnetic bead and the suspending medium,  $\Delta\chi_b$ , is replaced with a difference between an averaged magnetic susceptibility over the entire cell, or particles, and the suspending medium,  $\Delta\chi_c$ . With this assumption, and a force balance on a particle, Eqs. (2–5) were solved to obtain

$$\Delta\chi_c = \mu_o \frac{9\eta v_c}{2r_c^2 + g\Delta\rho} \frac{1}{\frac{1}{2} |\nabla \mathbf{B}^2|}, \quad (6)$$

where  $r_c$  is the diameter of the particle (cell). With respect to immunomagnetically labeled cells, the use of this relationship effectively reports a magnetic susceptibility which is averaged over the entire volume of the particle or cell.

### Quantification of Magnetic Susceptibility

Currently, there exists no practical way to accurately quantify the magnetic susceptibility,  $\Delta\chi$ , of a large number of paramagnetically labeled cells both in terms of a mean and distribution. However, there are reports of several different techniques that have been used to either measure or approximate the magnetic susceptibility of small particles or labeled cells. An early technique is one reported by Gill et al. (1960). This technique used an instrument in which the movement of an aqueous suspended particle or cell in an experimentally measured magnetic energy gradient was determined. The measurement of the particle velocity was determined through visual, microscopic observations and the use of a stopwatch. With this apparatus, measurements were made of polystyrene latex beads and red blood cells. Winto-Morbach et al. (1994, 1995) developed a technique which they refer to as "magneto-cytometry," which is similar to the technique of Gill et al. (1960) In this technique, erythrocytes (paramagnetic) or magnetically labeled human leukemia cells (REH and K562), contained within a small capillary tube, are placed in a high magnetic field gradient created by an electromagnet. By microscopically determining the number of cells disappearing from the field of view after turning on the magnet, the fraction of the magnetic cells can be determined. From this fraction, and using Scatchard analysis, the authors propose to be able to determine the number of bound labels per cell. However, this work is preliminary and a number of significant issues must be addressed. First and most importantly, their instrument does not measure cell velocities, but only the fraction of magnetic cells relative to the total number of cells. Therefore, one cannot directly determine the mean or distribution of the magnetic susceptibility of paramagnetically labeled cells, or indirectly, the receptor density. Second, to determine accurate values of the mean and distribution of the magnetic susceptibility of immunomagnetically labeled cells, a large number of cells need to be evaluated. A typical FACS histogram contains the results of  $10^4$  cells. Consequently, without computer automation, the use of the magneto-cytometry device and that of Gill et al. (1960) is limited to a few hundred cells (Winto-Morbach, 1996, 1995, 1994). Third, in the reports on the magneto-cytometer device, the authors do not report values for the  $\frac{1}{2}\nabla B^2$ . Based on the design reported, the values of  $\frac{1}{2}\nabla B^2$  are highly non-linear and rapidly increase as one moves closer to the pole piece. Without highly accurate maps of  $\frac{1}{2}\nabla B^2$ , only rough estimates of the magnetic susceptibility of a labeled cell can be made.

Zborowski et al. (1995) reported on studies in which mean measurements of the magnetic susceptibility of immunomagnetically labeled cells were determined. In this

system, immunomagnetically labeled cells flow through a region with a known, high magnetic energy gradient. Cells that are sufficiently immunomagnetically labeled are deflected and are deposited on the bottom surface of a glass surface in the flow channel. With the knowledge of the magnetic energy gradient and flow condition within the vessel, estimates can be made of the mean magnetic susceptibility of the labeled cells.

In a previously published paper (Reddy et al., 1996) we discussed a technique in which the mean and distribution of the magnetic susceptibility of populations of two different types of particles were determined. The two types of particles were Dynabeads, used for cell separation, and ion-exchange beads that bind the paramagnetic compound,  $\text{ErCl}_3$ . This technique, similar to that of both Gill et al. (1960) and Winto-Morbach (1994, 1995) uses microscopic observations of individual, suspended particles moving in a magnetic energy gradient. However, unlike those studies, these microscopic images were processed using a computer program, particle tracking velocimetry, PTV, which provided location and velocity data of individually tracked particles. A discussion of the application of this approach on a cell, called cell tracking velocimetry, CTV, is discussed in the previous publication in the series, "Quantification of Cellular Properties from External Fields and Resulting Induced Velocity: Cellular Hydrodynamic Diameter," by Chalmers et al. (1999a). A significant advantage of this method over all other techniques is that not only can velocity and location data be obtained for each cell or particle, but potential automation allows larger numbers of cells ( $>10^3$ ) to be processed.

In this paper, the second of a two-part series, we discuss the use of the CTV algorithm to determine the velocity of immunomagnetically labeled cells in a known magnetic energy gradient. As indicated in Eq. (6), if the values of  $\frac{1}{2}\nabla B^2$ , cell diameter, solution viscosity, and individual cell velocity are known, estimates can be made of the magnetic susceptibility of the immunomagnetically labeled cell. In the first paper in this series (Chalmers et al., 1999a) the process and limits of the quantification of the movement of cells due to gravity were presented. In this paper, the use of this quantification technique to measure the magnetic susceptibility of immunomagnetically labeled cells is discussed.

## EXPERIMENTAL METHODS

### Cells

The quantification of the movement of two types of immunomagnetically labeled cells will be presented: immunomagnetically labeled human lymphocytes and a human breast cancer cell line, MCF-7 (ATTC, Rockville, MD). The procurement and/or culturing of both of these cell lines have been discussed previously (Chalmers et al., 1998a,b; Sun et al., 1998).

## Immunomagnetic Labeling

The immunomagnetic labeling procedure used for these two cell types has also been previously published (Chalmers et al., 1998b; Sun et al., 1998) and will only briefly be discussed here. In summary, a two-step labeling protocol was used. First, a primary mouse antibody against the cell surface antigen of interest was allowed to bind to the cell. In the human lymphocyte case, the antibody was specific to the CD4 cell surface antigen and conjugated to the antibody was a fluorescein isothiocyanate (FITC) molecule (B-D Immunocytometry Systems, San Jose, CA). For the human breast cancer cell, the primary antibody was specific for epithelial membrane antigen (EMA) (Biomedica Corp., Foster City, CA). Next, the cells were labeled with a rat anti-mouse polyclonal antibody (pAb) conjugated to an iron dextran colloid (MACS microbeads, Miltenyi Biotec GmbH, Bergisch Gladbach, Germany).

## Experimental Apparatus

Figure 1a (taken from Reddy, 1996) presents a diagram of the flow channel and magnetic assembly. The magnetic field was created by two pairs of neodymium-iron-boron (Ne-Fe-B) magnets; each magnet had dimensions of  $2'' \times 2''$

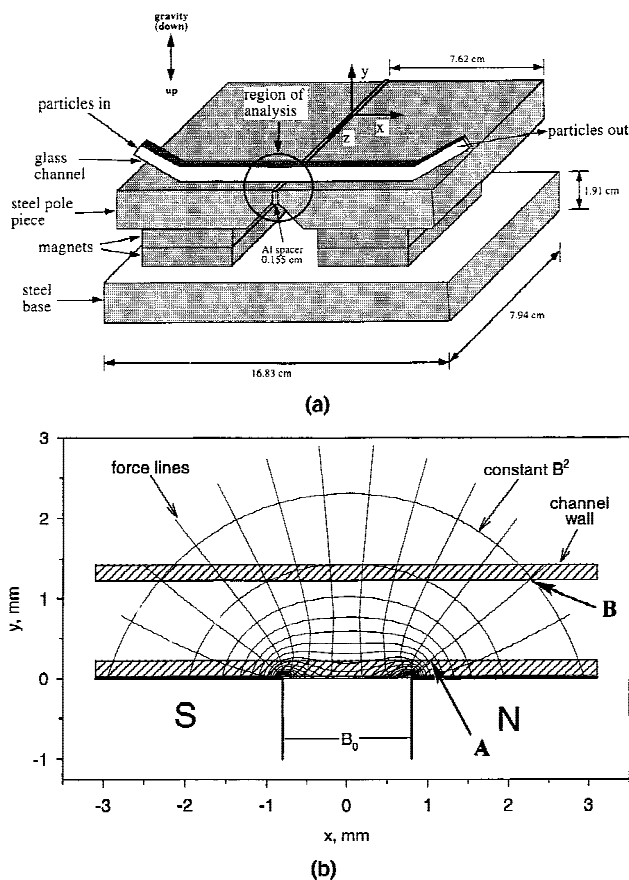


**Figure 1.** Diagram of the experimental apparatus (a) and an enlargement of the region in which cells are tracked (b). The force lines shown in b are based on computer simulations using experimentally determined constants.

$\times 1/2'' (W \times D \times H)$ . They were sandwiched between a steel base and two identical 1018 low-carbon cold-finished steel pole pieces. Magnetic flux is concentrated near the gap formed by the two pole pieces. An interpolar gap of 0.155 cm is created by an aluminum spacer. A square glass channel is attached to the top of the pole pieces. Magnetically labeled cells are pumped through tubing into the channel. The coordinate system originates on the top surface in the center of the gap. The edges of the pole pieces are at  $y = 0$  and  $x = \pm 0.0775$  cm. A square, borosilicate glass channel (nominally 1 mm I.D.  $\times$  1.4 mm O.D.) rests on the pole piece surfaces and is placed approximately 1 cm from the front face of the pole pieces. An enlargement of the highlighted region above and between the two pole pieces is presented in Fig. 1b. Overlaid on the physical geometry are lines of constant  $B^2$  and  $\nabla B^2$  lines, or force lines.

## Quantification of the Magnetic Field

Eqs. (4) and (5) suggest that for an induced dipole, the magnetic force lines are not coincident with the field lines. This differs from the simple case of the free electric charge. The physical interpretation of Eqs. (4) and (5) is that the force lines are proportional to the rate of change of field energy, proportional to  $B^2$ . For paramagnetic material this is the direction of steepest ascent of the  $B^2$  contours; for diamagnetic particles this is the direction of steepest descent (Zborowski, 1997). For the rectangular slot magnet used in these studies, the field analysis can be reduced to two dimensions provided the region of interest is far enough away from the front surface of the poles to neglect the edge effects characteristic of the third,  $z$ , dimension (see Fig. 1a,b).

Eq. (4) can be written in component form for magnetic migration along  $x$  and  $y$  coordinates. If we limit the analysis of cell migration to the  $y$  direction, then  $\nabla B^2$  of Eq. (5) and (6) reduces to  $dB^2/dy$ . The problem of mapping the field is complicated by the fact that even in the restricted region of viewing, the field and gradient change rapidly. Further, simple functional relationships equating field strengths with position do not exist for this geometry. The rather complex technique of conformal mapping of a line current onto an infinite slot has been applied (Zborowski, 1995). But this method results in errors due to the fact that the following underlying assumptions do not strictly hold: (1) the slot is infinitely deep and (2) the pole pieces have constant potential.

We have thus taken the approach of applying the CAE software program Magneto (Integrated Engineering Software, Winnipeg, Manitoba) to map the field. Magneto employs the boundary element method to evaluate the field for our time-invariant 2-D model. Because of geometrical non-uniformities in the third dimension—the effect of pole piece overhang (Fig. 1a) and the associated attenuation of the usable flux, as well as  $z$  component flux leakage, Magneto output must be calibrated against measured values. Experimental field measurements were made along the line of symmetry, in the center of the gap where  $x = 0$ , with a

Gauss meter and Hall effect probe (Model 9200 Gauss meter and STG920404 transverse probe, F.W. Bell, Orlando, FL). Magneto was then rerun with different specified values of the Ne-Fe-B magnet's residual induction until its output coincided with the field measurements. Maintaining a constant coercive force of  $-860,000$  A/m, convergence was reached with a residual induction of  $0.575$  T. This enabled the prediction of a saturation field inside the interpole gap,  $B_0$ , of  $1.7$  T (Fig. 1b).

With the magnetic parameters established for the Magneto model, the model was then used to output a grid of field values over the cell tracking region. The field values were then read by a Maple (Waterloo, Ontario) program and, using a five-point numerical differentiation formula,  $d\mathbf{B}^2/dy$  was computed at the grid nodes.

Figure 1b is a Maple-generated plot of  $\mathbf{B}^2$  contours, which define constant magnetostatic potential energy. Lines of magnetic force are orthogonal to the  $\mathbf{B}^2$  contours. These force lines, in the absence of any additional external force, define the trajectories of the paramagnetic cells in a stagnant fluid. As a point of reference, magnitudes of the y component of the magnetic force, at either end of one of these trajectory lines, points A and B in Fig. 1b, are  $3.629$  and  $0.213$  T<sup>2</sup>/mm, respectively. Since cells have a higher density than their suspending medium, these trajectory lines are modulated slightly by the effect of the gravity and buoyant forces. (The force—and the magnetic cell velocity—rapidly increase as the corners of the rectangular poles are approached.)

Position vectors obtained from particle tracking analysis were read into another Maple program which interpolated between the  $d\mathbf{B}^2/dy$  nodes to give the magnetic force component for any particle position. Inclusion of this value in Eq. (6) gave the solution of  $\Delta\chi$  for each cell at each video frame at which it was tracked. Since the magnetic susceptibility is an intrinsic property of the cell, provided the magnetizing field,  $\mathbf{H}$ , is not so large as to saturate the paramagnetic material of the label, the cells magnetic susceptibility should not change with position. Computing the susceptibility over the tracking range provides an internal check of the technique.

### Cell Location and Velocity Identification

A combination of microscopic observations, video recording, computer imaging, and the CTV algorithm, were used to quantify the movement of immunomagnetically labeled cells in the magnetic energy gradient. A more complete discussion of this technique can be found in the companion paper (Chalmers et al., 1999a).

## RESULTS

### CELL VELOCITIES

Figure 2 is a histogram of the fraction of the cell population with a given velocity versus the cell velocity (mm/s), on a

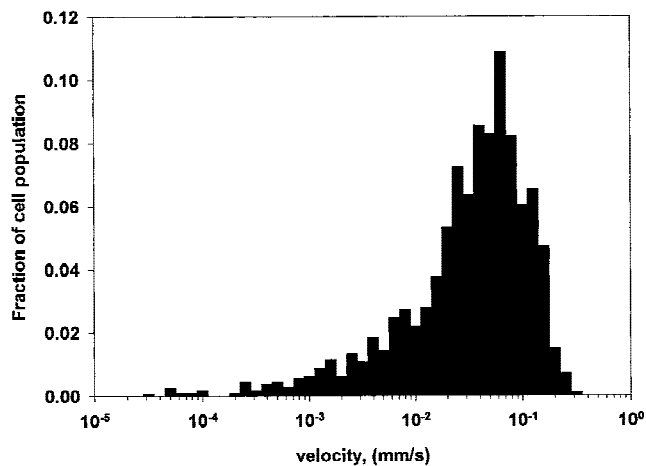


**Figure 2.** Histograms of the fraction of cell populations ( $n = 1147$ ) with a given velocity (mm/s) for immunomagnetically labeled human lymphocytes in the magnetic energy gradient.

log scale, for immunomagnetically labeled human lymphocytes in the magnetic energy gradient. The 1147 individual velocity data points used to make this histogram are actually each an average, ranging from a minimum of five velocity measurements, to up to 100, depending on the number of frames an individual cell was tracked. For comparison, Fig. 3 is a histogram ( $n = 637$ ) of the distribution of settling velocities of nonlabeled human lymphocytes. This velocity data was also presented in the previous paper in the series (see Fig. 7 in Chalmers et al. (1999a)).

As was discussed previously, the magnetic energy gradient in the apparatus used in this research is highly nonlinear. In addition, the magnetic energy gradient monotonically increases as either of the two pole pieces are approached. Consequently, a magnetically labeled cell will experience an increasing, attractive magnetic force as it approaches a pole. This increasing force is manifested by an increasing velocity as the cell approaches the pole piece and can be

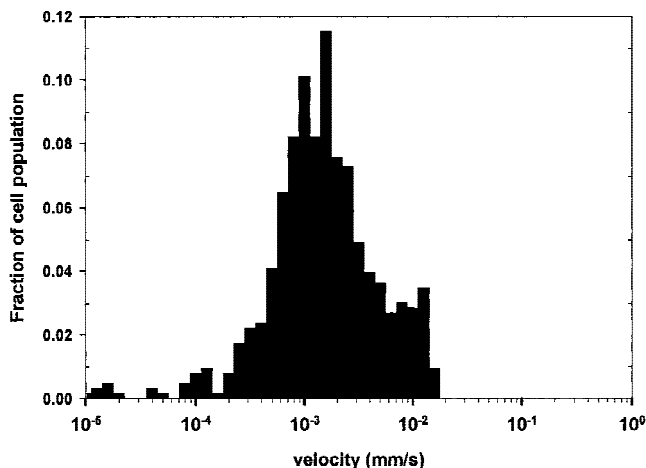


**Figure 3.** Histogram of the fraction of cell population ( $n = 637$ ) with a given velocity (mm/s) for nonlabeled human lymphocytes.

visually observed (data not shown). In contrast, for the data presented in Fig. 3 the driving force for the movement of the cells is gravity, which is constant. This constant force should result in a constant cell settling velocity which was experimentally observed.

The magnetic susceptibility,  $\Delta\chi$ , of immunomagnetically labeled human lymphocytes presented in Fig. 2 was determined by using the velocity data along with the corresponding position data, the magnetic energy gradient map, and Eq. (6). These measurements of  $\Delta\chi$  are presented in Fig. 4, again, in the form of a histogram as the fraction of cell population with a specific value of  $\Delta\chi$ . As in Fig. 2, each specific data point is the average value of  $\Delta\chi$  for a particular cell, the average ranging from a minimum of five measurements up to 100 for each individual cell.

The magnetic susceptibility of immunomagnetically labeled breast cancer cells, MCF-7, was also determined. As with the other data, a histogram is used to present the data ( $n = 1166$ ) in Fig. 5.

## DISCUSSION

The results presented above demonstrate the ability of the combination of a specialized instrument, computer imaging, and computer algorithms to determine, on a cell-by-cell basis, the magnetic susceptibility of immunomagnetically labeled cells. Such a cell-by-cell analysis provides both a mean and a distribution of  $\Delta\chi$  for a cell population. If one makes the assumption of a proportionality between the number of immunomagnetic labels bound to a cell and the number of cell surface markers on the cell, then this distribution in immunomagnetic susceptibility is also a measure of the distribution in the cell surface marker number. Technically, this distribution is also a function of the distribution in cell diameter (radius) and any distribution in the volume of the magnetic beads. A more complete discussion of the effect of cell size distribution can found in Chalmers et al. (1998a).

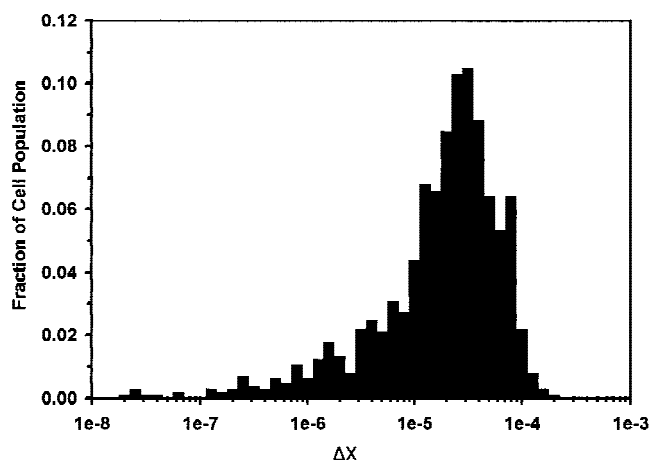


**Figure 4.** Histogram of the fraction of cell population ( $n = 1147$ ) with a given magnetic susceptibility,  $\Delta\chi$ , for the same cells presented in Fig. 2.

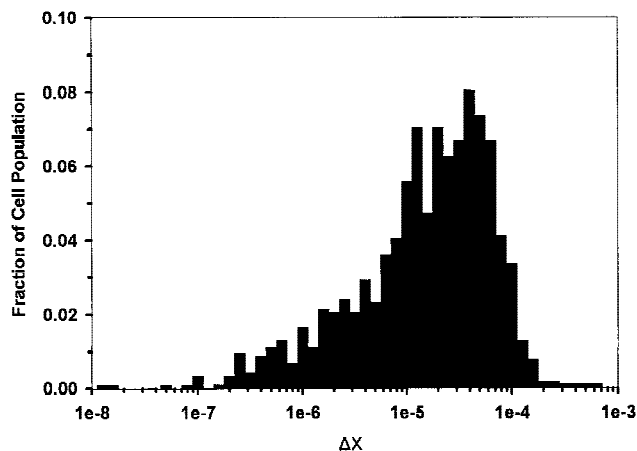


**Figure 5.** Histogram of the fraction of cell population ( $n = 1166$ ) with a given magnetic susceptibility,  $\Delta\chi$ , for breast cancer (MCF-7) cells.

A significant question with the technique described in this paper is the degree of accuracy of the calculated magnetic susceptibility for each tracked cell. There are four major sources of experimental error in the determination of magnetic susceptibility: an inaccurate magnetic energy gradient map, the uncertainty with respect to the position of the magnetic energy reference points, random error in the ability of the code to calculate the magnetically induced velocity, and random error in the ability of the code to determine the location of the cell (this error could be related to error in velocity determination also). An inaccurate magnetic energy gradient map, or a shift in reference points of an accurate map, should result in a systematic increase or decrease in the calculated magnetic susceptibility in a specific cell as it is tracked over a significant number of frames. This did, in fact, occur in earlier work before more accurate magnetic energy gradient maps were used (not presented). Other errors would result from random variation of the calculated magnetic susceptibility of an individual cell as it is tracked over many frames.

As discussed in the results section, the magnetically induced velocity in this apparatus is a strong function of the location of the cell. The closer to the magnetic pole tip, the higher the magnetic force acting on the cell, which in turn results in larger velocities (which was also visually observed). Consequently, an immunomagnetically labeled cell will accelerate as it moves closer to the pole tip (point A in Fig. 1b). However, unlike the velocity of immunomagnetically labeled cells, the magnetic susceptibility of a cell theoretically is not a function of location in our system. Therefore, a measure of the accuracy of this technique is the variability of the calculated magnetic susceptibility of a specific cell from frame to frame. Since the CTV algorithm provides velocity and location data for each tracked cell from a sequence of frames, which corresponds to specific time increments, it is possible to calculate an average magnetic susceptibility and a standard deviation over the frames the cell was tracked. The average magnetic susceptibilities were used to create the histograms in Figs. 4 and 5. Figure

6 is a scatter plot ( $n = 1147$ ) of the standard deviation of the average magnetic susceptibility versus the average  $\Delta\chi$  for human lymphocytes, and Fig. 7 is the same type of plot ( $n = 637$ ) for the MCF-7 cells. Note that the  $x$  axis is logarithmic with the same scale used in Figs. 4 and 5. This type of plot allows one to observe the range of the standard deviation for a given value of  $\Delta\chi$ .

Several observations and points can be made from Figs. 6 and 7. First, the standard deviation of the average values of  $\Delta\chi$  does not significantly change as the value of  $\Delta\chi$  changes. However, there appears to be a slight upward trend with higher  $\Delta\chi$ . We observed when earlier, less accurate, maps of the magnetic energy gradient were used, significant increases in standard deviation of  $\Delta\chi$  were observed with increasing values of  $\Delta\chi$ . This is not surprising due to the highly nonlinear nature of the magnetic energy gradient. As discussed previously, the magnetic energy gradient varied by a factor of 17 over a representative theoretical trajectory (point B to point A in Fig. 1b). Second, while the number of frames that the cell is tracked varied from 5 to 100, the distribution of frames tracked was random over the full range of  $\Delta\chi$ . Third, the range of standard deviation is higher with the MCF-7 cells when compared with the human lymphocytes. As was reported in the previous paper in this series (Chalmers et al., 1999a), both the size and the distribution in cell size is greater with the MCF-7 cells than the lymphocytes. We have observed that this increase in both size and distribution contributes to an increase in error in the algorithms ability to locate the center of the cell, which correspondingly, contributes to greater variation in calculated cell velocities.

To reduce one of the sources of potential error in the determination of magnetic susceptibility, we have developed and recently reported (Chalmers et al., 1999b) a new magnet design in which the region of cell motion has a nearly constant magnetic energy gradient. This simplifies the expression for the magnetic susceptibility, Eq. (6), to

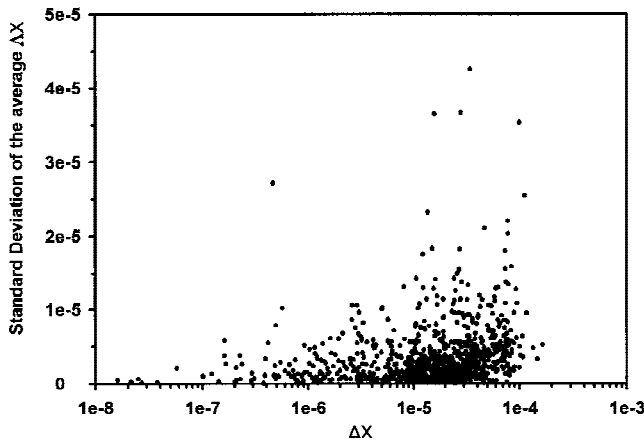


**Figure 6.** Standard deviation of a sequences of measurements of magnetic susceptibility, for each cell tracked, versus the mean of that sequence. The number of measurements in the sequence, (number of frames in which the cell was tracked), varied from 5 to about 100. This figure presents the measurements of the immunomagnetically labeled human lymphocytes.

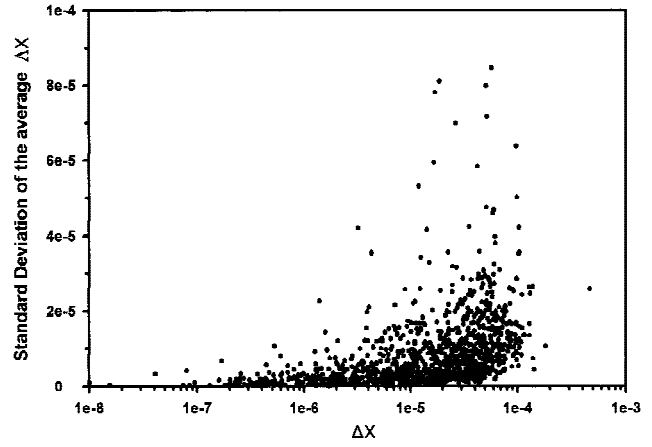


**Figure 7.** Standard deviation of a sequences of measurements of magnetic susceptibility, for each cell tracked, versus the mean of that sequence for breast cancer (MCF-7) cells. As in Fig. 6, the number of measurements in the sequence varied from 5 to about 100.

dividing the cell velocity by a constant magnetic energy gradient and, theoretically, eliminates the error associated with the determination of the exact cell location with respect to the magnetic energy gradient. Experimentally, any increase or decrease in the cell velocity in the direction of constant magnetic energy gradient is then an indication of a variation of the theoretically constant magnetic energy gradient.

In a previous publication (Chalmers et al., 1998a) we discussed the implications that a distribution in cell diameters has on one's ability to separate a cell population into different fractions based on the cells magnetic susceptibility. A relationship was developed, using "theoretical plate" analogies, to relate the number of "plates",  $n$ , or fractions, into which a population of cells can be divided. This relationship is based on the cell surface marker density,  $\alpha$ , or magnetically induced velocity,  $v$ , the nondimensionalized standard deviation,  $\sigma^*$ , of the cell diameters relative to the mean, and a term,  $z$ , which is a statistical term which defines the degree of certainty that each fraction is distinct. This relationship is given by

$$n = \frac{\ln\left(\frac{\alpha_n^*}{\alpha_0^*}\right)}{\ln\left(\frac{1+z\sigma^*}{1-z\sigma^*}\right)} = \frac{\ln\left(\frac{v_n^*}{v_0^*}\right)}{\ln\left(\frac{1+z\sigma^*}{1-z\sigma^*}\right)}; |z\sigma^*| < 1. \quad (7)$$

If one makes the assumption that the magnetic susceptibility,  $\Delta\chi$ , is proportional to the cell surface marker density,  $\alpha$ , the range of magnetic susceptibility reported in this paper, can be used to define the theoretical number of fractions into which the two cell populations used in this study could be "fractionated".

Chalmers et al. (1998a) reported the values for  $\sigma^*$  for human lymphocytes and MCF-7 cells to be 0.051 and 0.352, respectively. Figure 4 indicates that the range of  $\Delta\chi$  with significant numbers of cells to be  $1 \times 10^{-7}$  to  $2 \times 10^{-4}$ , or a

maximum to minimum  $\Delta\chi$  of 2000 for human lymphocytes, and Fig. 5 indicates a range of  $\Delta\chi$  of  $2 \times 10^{-7}$  to  $7 \times 10^{-4}$ , or a maximum to minimum  $\Delta\chi$  of 3500 for MCF-7 cells. Using a value of  $z\sigma^* = 0.102$  (Chalmers et al., 1998a), Eq. (7) indicates that one can theoretically “fractionate” a population of immunomagnetically human lymphocytes into 48 fractions, and with a value of  $z\sigma^* = 0.704$ , one can separate immunomagnetically labeled MCF-7 cells into 6 fractions. Recently, Chalmers et al. (1998b) and Moore et al. (1998) reported on a device in which fractionation of a population of cells based on a distribution of magnetic susceptibility can be achieved.

In this paper and the companion paper (Chalmers et al., 1999a), we have discussed the use of external fields, either gravity or magnetic energy gradient, microscopic imaging, and computer algorithms to measure cellular properties on a cell by cell basis. These two reports present results obtained with the use of a novel, analytical device. We are currently improving the magnetic energy gradient, the microscopic imaging, and computer algorithms. With these improvements, we believe it will be possible to combine the measurement of cell size and magnetic susceptibility at the same time on the same cell. This will allow measurements of cell surface marker density to be made on a cell-by-cell basis. In addition, improvements in the imaging and computer algorithms will improve the speed of the analysis.

This improved apparatus will allow us to address a number of important questions with respect to immunomagnetic labeling and, correspondingly, immunomagnetic separations. Some of these questions include the binding kinetics of antibody–magnetic colloids, possible internalization of magnetic labels, and possible cell–cell interactions, such as “drafting” effects when a sufficiently high concentration of immunomagnetic cells is used.

The authors express their thanks to the National Science Foundation (Grant No. BCS 9258004), the National Institutes of Health (Grant No. CA 62349), and the Whitaker Foundation (Grant No. 20010308) for their financial support.

## References

- Bertolini F, Thomas T, Battaglia M, Gibelli N, Pedrazzoli P, Robustelli Della Cuna G. 1997. A new “two-step” procedure for 4.5 log depletion of T and B cells in allogeneic transplantation and of neoplastic cells in autologous transplantation. *Bone Marrow Transplantation* 19: 615–619.
- Busch J, Huber P, Pfluger E, Miltenyi S, Holtz J, Radbruch A. 1994. Enrichment of fetal cells from maternal blood by high gradient magnetic cell sorting (double MACS) for PCR-based genetic analysis. *Prenatal Diagnosis* 14:1129–1140.
- Chalmers JJ, Mandal S, Fang B, Sun L, Zborowski M. 1998a. Theoretical analysis of cell separation based on cell surface marker density. *Biotechnol Bioeng* 59:10–20.
- Chalmers J, Sun L, Moore L, Zborowski M. 1998b. Immunomagnetic cell separation. *Biotechnol Progr* 14:141–148.
- Chalmers JJ, Zborowski M, Haam S, Zhou Y, McCloskey K, Moore L, Williams, PS. 1999a. Quantification of cellular properties from external fields and resulting induced velocity: Cellular hydrodynamic diameter. *Biotechnol Bioeng* XX:000–000.
- Chalmers J, Zhao Y, Nakamura M, Melnik K, Lasky L, Moore L, Zborowski M. 1999b. An instrument to determine the magnetophoretic mobility of paramagnetic particles and labeled, biological cells. *J Magn Magn Mater*. In press.
- Collins P, Watts M, Brocklesby M, Gerritsen B, Veys P. 1997. Successful engraftment of haploidentical stem cell transplant for familial haemophagocytic lymphohistiocytosis using both bone marrow and peripheral blood stem cells. *Br J Haematol* 96:644–646.
- Gard AL, Maughon RH, Schachner M. 1996. In vitro oligodendroglial properties of cell adhesion molecules in the immunoglobulin superfamily: Myelin-associated glycoprotein and N-CAM. *J Neurosci Res* 46:415–426.
- Gee AP, Mansour V, Weiler M. 1989. T-cell depletion of human bone marrow. *J Immunogenet* 16:103–115.
- Gill SJ, Malone CP, Downing M. 1960. Magnetic susceptibility measurements of single small particles. *Rev Sci Instrum* 31:1299–1303.
- Madison DL, Kruger WH, Kim T, Pfeiffer SE. 1996. Differential expression of rab3 isoforms in oligodendrocytes and astrocytes. *J Neurosci Res* 45:258–268.
- Miltenyi S, Muller W, Weichel W, Radbruch A. 1990. High gradient magnetic cell separation. *Cytometry* 11:231–238.
- Moore LR, Zborowski M, Sun L, Chalmers JJ. 1998. Lymphocyte fractionation using immunomagnetic colloid and dipole magnet flow cell sorter. *J Biochem Biophys Methods* 37:11–33.
- Radbruch A, Mechtold B, Thiel A, Miltenyi S, Pfluger E. 1994. High-gradient magnetic sorting. *Methods Cell Biol* 42:387–403.
- Reddy S, Moore L, Zborowski M, Chalmers JJ. 1996. Determination of the magnetic susceptibility of labeled particles by video imaging. *Chem Eng Sci* 51:947–956.
- Schmitz B, Radbruch A, Kummel T, Wickenhauser C, Korb H, Hansmann ML, Thiele J, Fischer R. 1994. Magnetic activated cell sorting (MACS)—A new immunomagnetic method for megakaryocytic cell isolation: Comparison of different separation techniques. *Eur J Hematol* 52:267–275.
- Shapiro H. 1995. *Practical flow cytometry*. New York: John Wiley & Sons. p 1.
- Sun L, Zborowski M, Moore L, Chalmers JJ. 1998. Continuous, flow-through immunomagnetic cell separation in a quadrupole field. *Cytometry* 33:469–475.
- Vogel W, Behringer D, Scheduling S, Kanz L, Brugger W. 1996. Ex vivo expansion of CD34+ peripheral blood progenitor cells: Implications for the expansion of contaminating epithelial tumor cells. *Blood* 88: 2707–2713.
- Winto-Morbach S, Tchikov V, Muller-Ruchholtz W. 1994. Magnetophoresis. I. Detection of magnetically labeled cells. *J Clin Lab Anal* 8: 400–406.
- Winto-Morbach S, Tchikov V, Muller-Ruchholtz W. 1995. Magnetophoresis. II. Quantification of iron and hemoglobin content at the single erythrocyte level. *J Clin Lab Anal* 9:42–46.
- Winto-Morbach S, Tchikov V, Treumer J, Muller-Ruchholtz W. 1996. Measuring cell subpopulations recognizable with magnetic microspheres. 1st International Conference and Clinical Applications of Magnetic Carriers, Rostock, FRG, Sept. 5–7.
- Zborowski M. 1997. Physics of the magnetic cell sorting. In: Hafeli U, Schutt W, Teller J, Zborowski M, editors. *Scientific and clinical applications of magnetic microcarriers: An overview*. New York: Plenum Press. p 205–231.
- Zborowski M, Fuh CB, Green R, Sun L, Chalmers JJ. 1995. Analytical magnetophoresis of ferritin-labeled lymphocytes. *Anal Chem* 67: 3702–3712.